ISSN 2250-3153

Parallel Operation of Full Power Converters in Permanent-Magnet Direct-Drive Wind Power Generation System

B.Gavaskar Reddy, L.Maheswari, K.Rajagopal, K.Naga Jyothi

Abstract- Parallel operation is an effective way to improve the capacity of full power converter in permanent-magnet direct-drive (PMDD) wind power generation system. But it causes the zero-sequence circulating-current (ZSCC), which brings current discrepancy, current waveform distortion, power losses, and electromagnetic interference (EMI), etc. The paper proposes a new topology of full power converters which are composed of n full power converters. The n converters have the same structures and are in parallel with each other. Besides, the average models of the system are analyzed and the fundamental mechanism of ZSCC generation is given. Based on the above analysis, the control strategy of the system is designed. The simulation and experiment results of two parallel full power converters show the feasibility of the proposed theory and control scheme.

Index Terms- full power converters, parallel operation, wind power generation, zero-sequence circulating-current (ZSCC).

I. INTRODUCTION

WITH the development of wind power generation technology, the power rating of wind turbine is becoming larger and larger and some have got to the level of 10 MW [1]–[4]. In the permanent-magnet direct-drive (PMDD) wind power generation system, the generator is connected to the line through the full power converter [5]–[7]. Being limited by the power rating of switching devices, it is difficult to transmit the large power to the line through single converter. To overcome this problem, the parallel operation of converters is studied [8]–[10].

Without the current pressure increase of single switching device, the parallel operation can increase the total current effectively, which makes it possible to manufacture higher power rating converters. When the capacity of wind turbine is constant, the switching devices with lower power rating can be used to reduce the cost through the parallel operation. Meanwhile, the parallel operation makes module design convenient to shorten the production period and widen the application field of power module [11]–[17]. Furthermore, the harmonics of total current can be reduced greatly through carrier phase shifted (CPS). Consequently, the power rating of filter can be decreased to reduce the production cost. At last, the parallel operation can realize redundancy design of N+1 to improve the system reliability [18]–[23].

There is no zero-sequence circulating-current (ZSCC) in the system with single converter because the ZSCC route does not exist. But it is serious in the parallel system if the ZSCC route exists [8], [10], [24]. The ZSCC is caused by the character differences of the parallel converters, such as inductor, switching device, switching frequency, dead-time, load, etc. But these are the apparent reasons. The intrinsic reason of ZSCC generation should be analyzed, because it is useful for us to understand the ZSCC generation mechanism and suppress the ZSCC. The ZSCC only flows among the parallel converters, which increases the power loss, decreases the system efficiency, and shortens the life of switching devices. Moreover, the ZSCC can induce current discrepancy, which makes the current pressures of switching devices different. Therefore, the capacity increase of the total system is limited [25], [26]. The ZSCC distorts the three-phase currents and increases the total harmonic distortion (THD), which causes pollution to the line. Besides, the high frequency components of ZSCC can cause the serious problem of electromagnetic interference (EMI). There are mainly two ways to eliminate the ZSCC. On the one hand, it can be eliminated by breaking the ZSCC route. On the other hand, it can be depressed by proper control methods [12], [27], [28]. The former way is used traditionally. In [29], the isolation transformer is used to break the ZSCC route and eliminate the ZSCC. Moreover, some special harmonics can be eliminated through CPS or the different structures of second sides of transformer to reduce the pollution to the line. But the isolation transformer usually operates at the line frequency and its volume and weight are large, which increases the production cost. Therefore, this method is not suitable for the MW-level PMDD wind power system. In [30], the topology with separate dc buses is proposed, which breaks the ZSCC route and

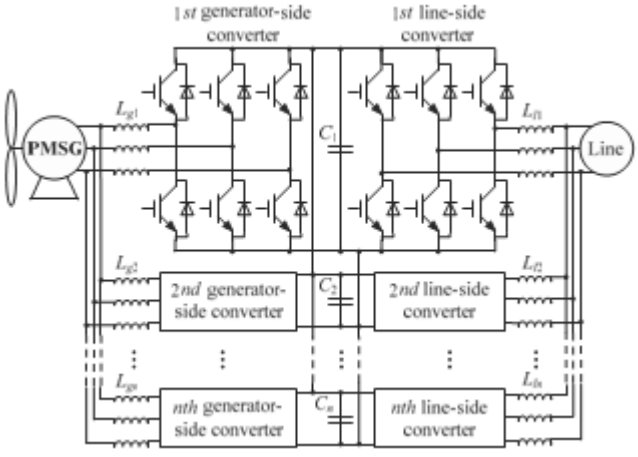

Fig. 1. System topology

eliminates the ZSCC. But this topology is only suitable for special generators with isolation windings. When the common three-phase generator is used, the problem of ZSCC is still very serious because the generator-side ZSCC and the line-side ZSCC are coupled with each other. So the application field of this

topology is limited. Furthermore, the separation of dc buses enlarges the system volume and is inconvenient for module design. In addition, the two dc bus voltages must be both controlled, which requires more voltage sensors and makes the control system complicate. References [31], [32] control the parallel converters as one converter to depress the ZSCC. But this kind of control method is too complicated to realize parallel operation with multimodules. In [12], the ZSCC is suppressed via null-vector duty. But it needs to change the conventional space vector pulse width modulation (SVPWM) strategy, which makes it complicate to achieve and limits its application scope.

To overcome the above problems, the paper proposes a new topology of PMDD wind power system. Its average models and ZSCC phenomenon are analyzed. It is found that the generator-side ZSCC and the line-side ZSCC are independent with each other. Besides, the intrinsic reason of ZSCC generation is the discrepancy of the zero-axis duty cycles for the parallel converters. According to the above analysis, the ZSCC controllers are designed, which depress the generator-side ZSCC and the line-side ZSCC effectively and do not increase the hardware cost. Moreover, they do not change the conventional SVPWM strategy, which makes them easier to achieve and expands their application scope. The problems caused by ZSCC, such as current discrepancy, current waveform distortion, etc., are overcome well and the reliability and efficiency of the system are improved. The proposed topology of the wind power system is described in Section Ⅱ. The ZSCCs of the system are analyzed in three-phase stationary coordinates and synchronous rotating coordinates respectively in Section Ⅲ. The control strategy is presented in Section Ⅳ. The simulation and experimental results separately verify the validity of the theoretical analysis

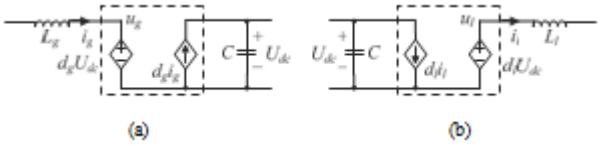

Fig. 2. Average model of single phase bridge. (a) Generator – side (b) Line - side

and control strategy in Sections Ⅴ and Ⅵ. Finally, some conclusions are given in Section Ⅶ.

II. SYSTEM TOPOLOGY

The proposed topology is illustrated in Fig. 1. Each converter is the back-to-back two-level voltage-source converter (VSC) and n converters with the same structures are paralleled, which have the common dc bus. The generator is the common three-phase permanent magnet synchronous generator (PMSG). Ck (k=1, 2, … , n) is the dc bus capacitor. Lgk (k=1, 2, … , n) is the three-phase inductance of generator-side, which has the function of filtering and avoiding the shortness of dc bus. Llk (k=1, 2, … , n) is the three-phase inductance of line-side, which can filter the harmonic, store energy, and avoid the shortness of dc bus. Increasing the inductances can suppress the high frequency components of the ZSCCs but can not suppress the low frequency components of the ZSCCs effectively. In addition, increasing inductances means the increment of volume, weight, and cost of the wind power converter. Therefore, the ZSCCs can not be only suppressed by increasing inductances.

III. ZSCC ANALYSIS

A. *ZSCC analysis in three-phase stationary coordinates*

The ZSCCs of the parallel system are analyzed through the average model. The inductance current i_L and the dc bus voltage U_{dc} can be treated as constant in a switching period because the period is very short commonly [12]. According to the average theory, the neutral point voltage of phase bridge u and the current of top switch i can be expressed as:

$$u = dU_{dc} \quad (1)$$

$$i = di_L \quad (2)$$

where d is the phase duty cycle. Then we can get the average model of single phase bridge on the generator-side and the line-side respectively, as shown in the dashed frames in Fig. 2, where the subscript g and l denote the generator-side and the line-side respectively.

According to the average model of single phase bridge, the average model of the parallel system can be got, as shown in Fig. 3, where the dashed circle part is the simple model of the PMSG; e_{ga}, e_{gb}, and e_{gc} are the electromotive forces (EMFs) of the PMSG; L_s and R_s are the leakage inductance and the resistance of the stator respectively; i_{gak}, i_{gbk}, and i_{gck} (k=1, 2, … , n) are the three-phase input currents on ac side of the kth

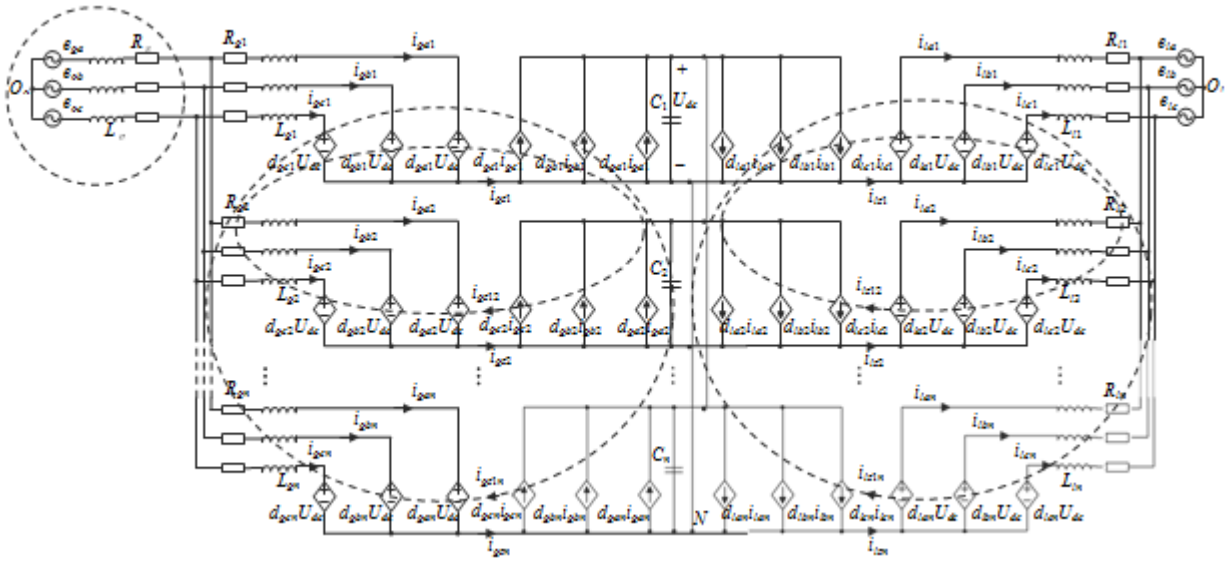

Fig. 3. Average model of the parallel system in three-phase stationary coordinates.

generator-side converter; d_{gak}, d_{gbk}, and d_{gck} (k=1, 2, … , n) are the three-phase duty cycles of the kth generator-side converter; R_{gk} (k=1, 2, … , n) is the equivalent series resistances (ESRs) of inductor for the kth generator-side converter; e_{la}, e_{lb}, and e_{lc} are the three-phase voltages of the line; i_{lak}, i_{lbk}, and i_{lck} (k=1, 2, … , n) are the three-phase output currents on ac side of the kth line-side converter; d_{lak}, d_{lbk}, and d_{lck} (k=1, 2, … , n) are the three-phase duty cycles of the kth line-side converter; R_{lk} (k=1, 2, … , n) are the ESRs of inductor for the kth line-side converter. Because there is no ZSCC route in single converter, the ZSCC is not generated even if the zero-sequence voltage exists. But the ZSCC routes exist in the parallel system and their resistances are small. Therefore, the serious ZSCC will be generated even if the zero-sequence voltage is small. In Fig. 3, i_{gzk} (k=1, 2, … , n) and i_{lzk} (k=1, 2, … , n) are the ZSCCs of the kth generator-side converter and the kth line-side converter respectively.

$$i_{gzk} = i_{gak} + i_{gbk} + i_{gck}, \ (k = 1, 2, \cdots, n) \qquad (3)$$

$$i_{lzk} = i_{lak} + i_{lbk} + i_{lck}, \ (k = 1, 2, \cdots, n) \qquad (4)$$

In the proposed topology, there are n-1 ZSCC routes for each converter. Taking the 1st generator-side converter for example, as shown in Fig. 3, the ZSCC between it and the kth generator-side converter is defined as igz1k. Therefore, its ZSCC, namely i_{gz1}, can be expressed as:

$$i_{gz1} = \sum_{i=2}^{n} i_{gz1i}. \qquad (5)$$

Similar conclusions can be got for the else generator-side converters and the line-side converters can be analyzed using the same method.

According to the Kirchhoff's voltage law and the average model as shown in Fig. 3, the voltage equations of the kth generator-side converter and the kth line-side converter can be expressed as follows respectively:

$$L_{\sigma}\frac{d}{dt}\begin{bmatrix} i_{ga} \\ i_{gb} \\ i_{gc} \end{bmatrix} + L_{gk}\frac{d}{dt}\begin{bmatrix} i_{gak} \\ i_{gbk} \\ i_{gck} \end{bmatrix} + R_s\begin{bmatrix} i_{ga} \\ i_{gb} \\ i_{gc} \end{bmatrix} + R_{gk}\begin{bmatrix} i_{gak} \\ i_{gbk} \\ i_{gck} \end{bmatrix} = \begin{bmatrix} e_{ga} - d_{gak}U_{dc} - U_{NO_g} \\ e_{gb} - d_{gbk}U_{dc} - U_{NO_g} \\ e_{gc} - d_{gck}U_{dc} - U_{NO_g} \end{bmatrix} \qquad (6)$$

$$L_{lk}\frac{d}{dt}\begin{bmatrix} i_{lak} \\ i_{lbk} \\ i_{lck} \end{bmatrix} + R_{lk}\begin{bmatrix} i_{lak} \\ i_{lbk} \\ i_{lck} \end{bmatrix} = \begin{bmatrix} -e_{la} + d_{lak}U_{dc} + U_{NO_l} \\ -e_{lb} + d_{lbk}U_{dc} + U_{NO_l} \\ -e_{lc} + d_{lck}U_{dc} + U_{NO_l} \end{bmatrix} \qquad (7)$$

Where

$$i_{ga} = \sum_{i=1}^{n} i_{gak}, \quad i_{gb} = \sum_{i=1}^{n} i_{gbk}, \quad i_{gc} = \sum_{i=1}^{n} i_{gck}. \qquad (8)$$

According to the Kirchhoff's current law and the average model as shown in Fig. 3, we can get the current equation of the system:

$$\sum_{i=1}^{n}\begin{bmatrix} d_{gai} \\ d_{gbi} \\ d_{gci} \end{bmatrix}^T\begin{bmatrix} i_{gai} \\ i_{gbi} \\ i_{gci} \end{bmatrix} = C\cdot\frac{dU_{dc}}{dt} + \sum_{i=1}^{n}\begin{bmatrix} d_{lai} \\ d_{lbi} \\ d_{lci} \end{bmatrix}^T\begin{bmatrix} i_{lai} \\ i_{lbi} \\ i_{lci} \end{bmatrix} \qquad (9)$$

Where

$$C = \sum_{i=1}^{n} C_i. \qquad (10)$$

B. ZSCC analysis in synchronous rotating coordinates

The average model in three-phase stationary coordinates should be transformed to one in synchronous rotating coordinates to simplify the controller design. The two-dimension coordinate transform, namely ab/dq transform, is usually used to control the

system in two dimensions and it is based on the premise that the sum of the three-phase currents is zero. The transform equation is as follows:

$$\begin{bmatrix} x_d \\ x_q \end{bmatrix} = \frac{2}{\pi} \begin{bmatrix} -\sin(\omega t - 2\pi/3) & \sin \omega t \\ -\cos(\omega t - 2\pi/3) & \cos \omega t \end{bmatrix} \frac{1}{\sqrt{3}} \begin{bmatrix} x_a \\ x_b \end{bmatrix} \quad (11)$$

where ω is the synchronous angular velocity.

In the parallel system, the d-axis and q-axis components obtained by (11) are not accurate due to the existence of ZSCCs. To get the accurate d-axis and q-axis components and the ZSCCs, the three-dimension coordinate transform, namely abc/dqz transform, is adopted:

$$\boldsymbol{T} = \frac{2}{3} \begin{bmatrix} \cos \omega t & \cos(\omega t - 2\pi/3) & \cos(\omega t + 2\pi/3) \\ -\sin \omega t & -\sin(\omega t - 2\pi/3) & -\sin(\omega t + 2\pi/3) \\ 1/\sqrt{2} & 1/\sqrt{2} & 1/\sqrt{2} \end{bmatrix}. \quad (12)$$

The relations between variables in three-phase stationary coordinates and ones in synchronous rotating coordinates can be expressed as:

$$\left[x_d \;\; x_q \;\; \frac{\sqrt{2}}{3} x_z \right]^T = \boldsymbol{T} \left[x_a \;\; x_b \;\; x_c \right]^T. \quad (13)$$

The d-axis and q-axis components can be got correctly by (12) and (13). But the three-phase currents of ac side are still distorted seriously if the ZSCCs are not controlled. At the same time, current discrepancy, EMI, etc. are generated. Therefore, the ZSCC controllers are needed to suppress the ZSCCs.

According to (6), (7), and (12), the voltage equations of the kth generator-side converter and the kth line-side converter in synchronous rotating coordinates can be expressed as follows respectively:

$$\begin{aligned} & L_\sigma \frac{d}{dt} \begin{bmatrix} i_{gd} \\ i_{gq} \\ i_{gz} \end{bmatrix} + L_{gk} \frac{d}{dt} \begin{bmatrix} i_{gdk} \\ i_{gqk} \\ i_{gzk} \end{bmatrix} + R_s \begin{bmatrix} i_{gd} \\ i_{gq} \\ i_{gz} \end{bmatrix} + R_{gk} \begin{bmatrix} i_{gdk} \\ i_{gqk} \\ i_{gzk} \end{bmatrix} + \\ & \begin{bmatrix} 0 & -\omega & 0 \\ \omega & 0 & 0 \\ 0 & 0 & 0 \end{bmatrix} \begin{bmatrix} i_{gdk} \\ i_{gqk} \\ i_{gzk} \end{bmatrix} + L_\sigma \begin{bmatrix} 0 & -\omega & 0 \\ \omega & 0 & 0 \\ 0 & 0 & 0 \end{bmatrix} \begin{bmatrix} i_{gd} \\ i_{gq} \\ i_{gz} \end{bmatrix} \\ & = \begin{bmatrix} e_{gd} - d_{gdk} U_{dc} \\ e_{gq} - d_{gqk} U_{dc} \\ e_{gz} - d_{gzk} U_{dc} - 3U_{NG} \end{bmatrix} \end{aligned} \quad (14)$$

$$\begin{aligned} & L_{lk} \frac{d}{dt} \begin{bmatrix} i_{ldk} \\ i_{lqk} \\ i_{lzk} \end{bmatrix} + R_{lk} \begin{bmatrix} i_{ldk} \\ i_{lqk} \\ i_{lzk} \end{bmatrix} + L_{lk} \begin{bmatrix} 0 & -\omega & 0 \\ \omega & 0 & 0 \\ 0 & 0 & 0 \end{bmatrix} \begin{bmatrix} i_{ldk} \\ i_{lqk} \\ i_{lzk} \end{bmatrix} \\ & \sum_{i=1}^{n} \begin{bmatrix} d_{gdi} \\ d_{gqi} \\ d_{gzi} \end{bmatrix}^T \begin{bmatrix} i_{gdi} \\ i_{gqi} \\ \frac{2}{9} i_{gzi} \end{bmatrix} = \frac{3}{2} C \frac{dU_{dc}}{dt} + \sum_{i=1}^{n} \begin{bmatrix} d_{ldi} \\ d_{lqi} \\ d_{lzi} \end{bmatrix}^T \begin{bmatrix} i_{ldi} \\ i_{lqi} \\ \frac{2}{9} i_{lzi} \end{bmatrix}. \end{aligned} \quad (15)\ (16)$$

In addition, the sums of the ZSCCs on the generator-side and the line-side are both zero:

$$\sum_{i=1}^{n} i_{gzi} = \sum_{i=1}^{n} i_{lzi} = 0. \quad (17)$$

According to (14)-(17), the average model of the parallel system in synchronous rotating coordinates can be got, as shown in Fig. 4. It can be seen that the ZSCCs of the generator-side and the line-side are independent with each other. The generator-side ZSCCs are caused by the discrepancy of zero-axis duty cycles for the parallel generator-side converters. The change of dgzk (k=1,2, … , n) has an influence on the generator-side ZSCCs. Besides, all the generator-side ZSCCs are equal to zero if n-1 ones are zero. Similarly, the conclusions about the line-side ZSCCs can be got. The ZSCCs of the generator-side and the line-side can be rewritten as:

$$\begin{aligned} & L_{g1} \frac{di_{gz1}}{dt} + R_{g1} i_{gz1} + d_{gz1} U_{dc} \\ & = L_{g2} \frac{di_{gz2}}{dt} + R_{g2} i_{gz2} + d_{gz2} U_{dc} \\ & \# \\ & = L_{gn} \frac{di_{gzn}}{dt} + R_{gn} i_{gzn} + d_{gzn} U_{dc} \end{aligned} \quad (18)$$

$$\begin{aligned} & L_{l1} \frac{di_{lz1}}{dt} + R_{l1} i_{lz1} - d_{lz1} U_{dc} \\ & = L_{l2} \frac{di_{lz2}}{dt} + R_{l2} i_{lz2} - d_{lz2} U_{dc} \end{aligned} \quad (19)$$

$$= L \quad \frac{di_{lzn}}{dt} + R \quad - d \quad U \quad .$$
$$i \quad ln \qquad ln\ lzn \qquad lzn \quad dc$$

IV. CONTROL STRATEGY

Fig. 5 shows the control strategy of the parallel PMDD wind power system and Fig. 6 is the detailed control strategy. The electrical rotor angular position of the PMSG θ g is got by the sliding-mode-observer (SMO), which has the high robustness and increases the reliability of the system [33]–[37]. Its output is provided to all of the generator-side converters. The SMO is contained in the 1st generator-side controller and its details are where ω g and ω l are the electrical rotor angular velocity of the PMSG and the synchronous angular velocity of the line respectively.

The current equation of the system in synchronous rotating coordinates can be got from (9) and (12) as follows: provided in Appendix. The kth (k=2, 3, … , n) generator-side controller has its own ZSCC controller whose principle is discussed below.

Except the SMO and the ZSCC controllers, the else parts of the generator-side controllers have no differences, which are described as follows.

For the kth (k=1, 2, … , n) generator-side converter, the three-phase currents igak, igbk, and igck are transformed into the d-axis and q-axis currents igdk and igqk to be as the feedbacks of the d-axis and q-axis current loops respectively. The q-axis

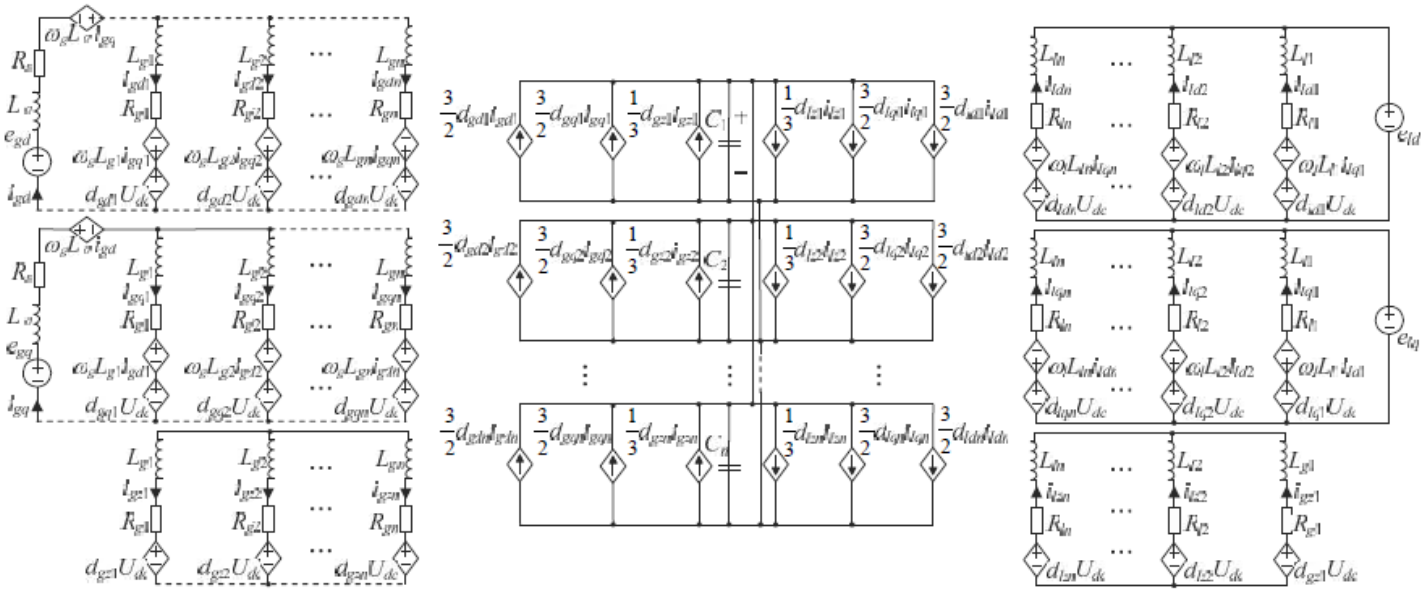

Figure 4: Average model of the parallel system in synchronous rotating coordinates.

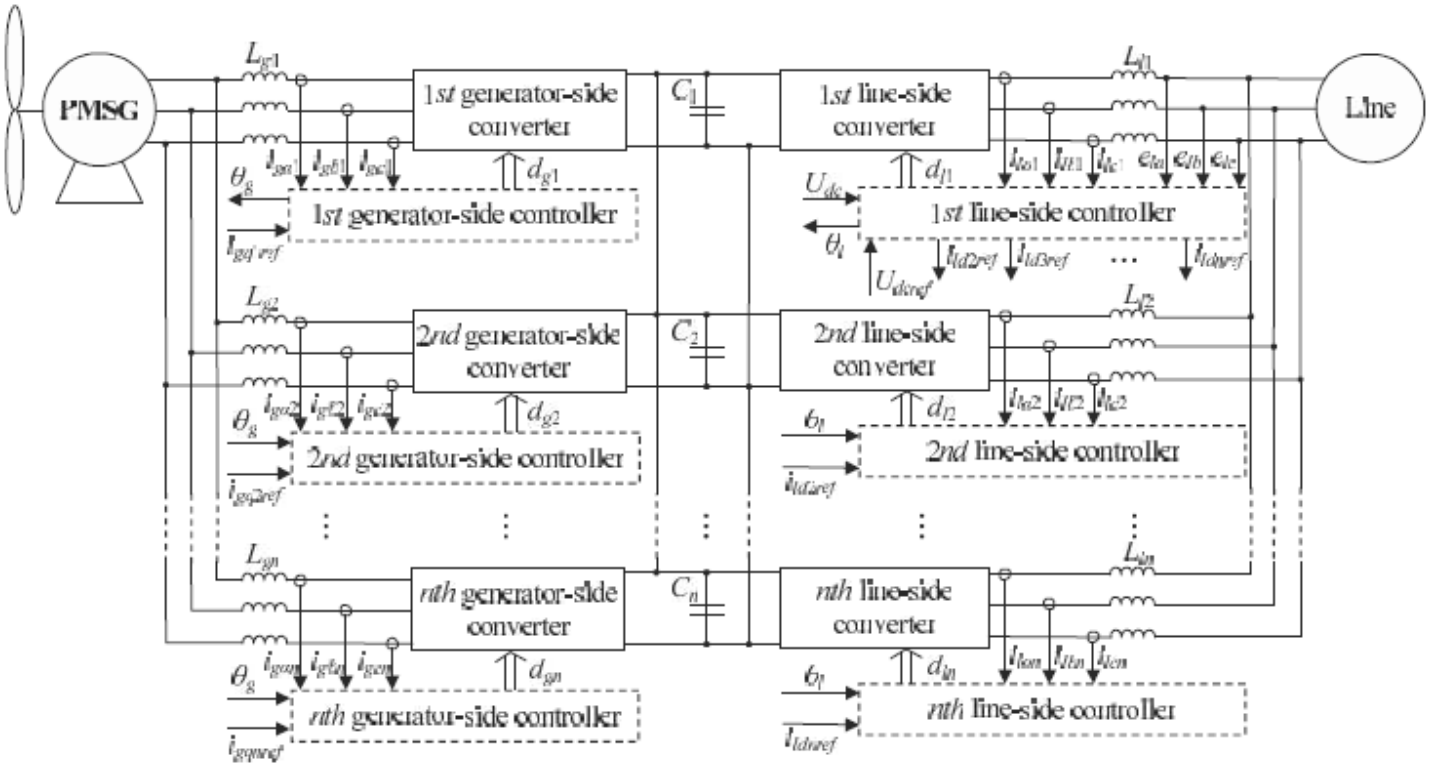

Figure 5: Control strategy of the system.

current reference, namely igqk, is given manually according to the torque reference. It should be noted that igqk is usually got by maximum power point tracking (MPPT) in wind farm to capture the wind power maximally. The d-axis reference, namely igdk, is usually zero to guarantee that the capability of transmitting power is maximum when the power capacity of converter is constant. The outputs of the d-axis and q-axis PI regulators are added to –ωgLgqigq and ωg(Lgdigd+Ψf) respectively to be as the d-axis and q-axis reference voltages, namely ugdk and ugqk, where Lgd and Lgq are the d-axis and q-axis inductances of the PMSG; Ψf is the amplitude of the flux induced by the permanent magnets of the rotor in the stator phases. Fig. 6 (c) and (d) is the detailed control strategy of the line-side converters. All of the line-side converters have the common dc voltage loop whose output is divided by weight to be as the d-axis current references of the line-side converters, namely ildkref (k=1, 2, … , n). The angular position of the line θl is got by the phase locked loop (PLL). The dc voltage loop and the PLL unit are contained in the 1st line-side controller. The kth (k=2, 3, … , n) line-side controller has its own ZSCC controller. Except the dc voltage loop, the PLL unit, and the ZSCC controllers, the else parts of the line-side controllers have no differences, which are described as follows.

The q-axis references, namely ilqk (k=1, 2, … , n), are usually zero to realize the line connection with unit power factor. The three-phase currents ilak, ilbk, and ilck are transformed into the d-axis and q-axis currents ildk and ilqk to be as the feedbacks of the d-axis and q-axis current loops respectively. The outputs of the d-axis and q-axis PI regulators are added to (eld–ωlLlkilqk) and (elq+ωlLlkildk) respectively to be as the d-axis and q-axis reference voltages, namely uldk and ulqk.

The key of the control strategy is the ZSCC controllers which are designed based on the above analysis, according to the theory of SVPWM. Because the ZSCCs of the generator-side and the line-side are independent with each

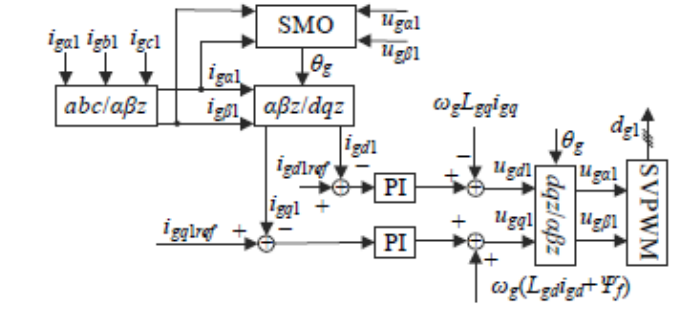

(a)

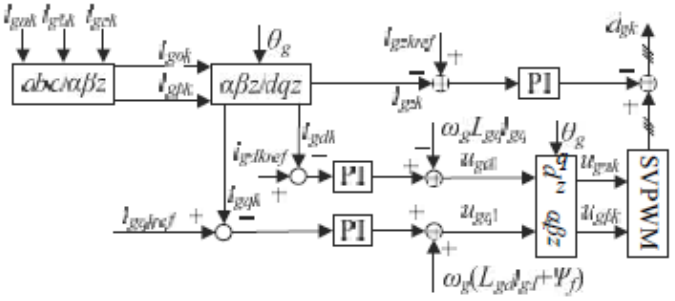

(b)

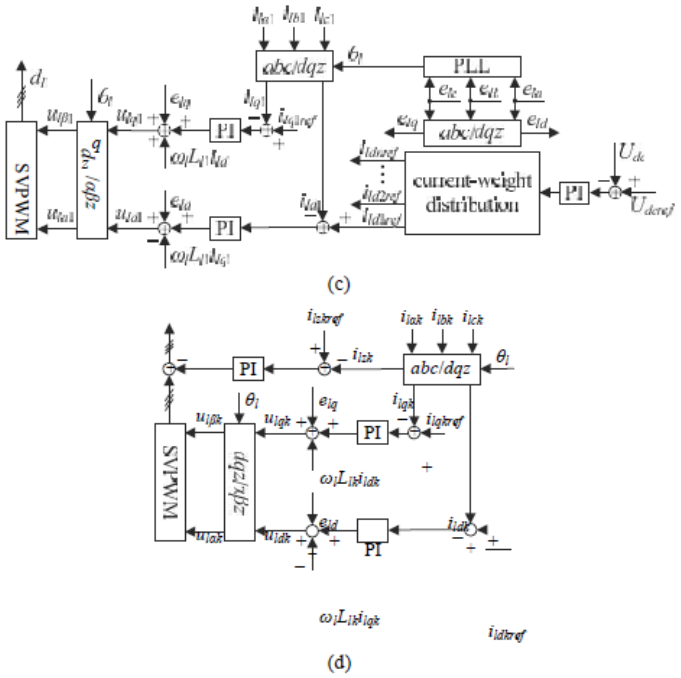

Fig. 6. Detailed control strategy. (a) The 1st generator-side converter. (b) The kth (k=2, 3, … , n) generator-side converter. (c) The 1st line-side converter. (d) The kth (k=2, 3, … , n) line-side converter.

other, the ZSCC controllers of the generator-side and the line-side can be designed independently.

Take the ZSCC controllers of the generator-side for example. To simplify the control system, we regulate igz2, igz3, … , igzn by changing dgz2, dgz3, … , dgzn respectively. If igz2, igz3, … , igzn are all suppressed, igz1 is suppressed automatically, due to (17). Firstly, the current sensors measure the three-phase currents igak, igbk, and igck (k=2, 3, … , n). According to (12) and (13), the zero-axis current igzk can be got, which is as the feedback of the kth ZSCC controller. And the reference value of the kth ZSCC controller is zero. After the PI regulation, the output Δdk is added to dgak, dgbk, and dgck respectively to regulate dgzk and suppress the generator-side ZSCCs, according to (18). Besides, the absolute value of Δdk should be less than T0/4. T0 is the time duration for which the null vectors U0 (000) and U7 (111) are applied. Take the sector contained by vectors U2 (010) and U3 (011) for example and presume that Δdk is positive, as shown in

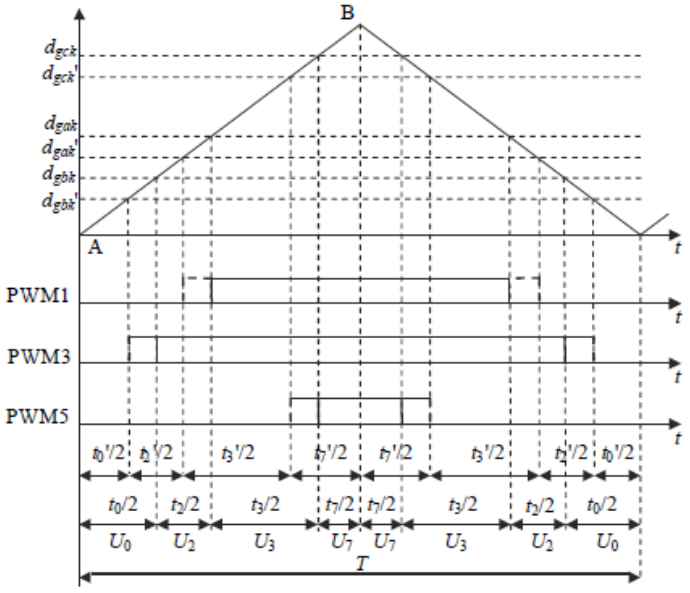

Figure 7: Regulation of PWM signals.

TABLE I
NOMINAL PARAMETERS OF PMSG

PARAMETER	Nominal value
rating frequency	26.67 Hz
rating voltage	230 V
rating power	10 kW
pole pairs	8
phase resistance of stator	0.45 Ω
synchronous inductance	0.005 H
flux amplitude of rotor	0.8 Wb

Fig. 7. The original PWM signals and the actual ones regulated by the ZSCC controller are indicated by the dashed lines and the solid lines respectively. The equations can be got:

$$t_2 = t_2', \quad t_3 = t_3' \tag{20}$$

$$t_0/2 - t_0'/2 = \Delta d_k/k_{AB}, \quad t_7/2 - t_7'/2 = -\Delta d_k/k_{AB} \tag{21}$$

where t2′, t3′, t0′, and t7′ are the original durations of vectors U2, U3 , U0 , and U7 respectively; t2, t 3, t 0, and t7 are the actual durations of vectors U2, U3, U0, and U7 respectively; kAB is the slope of line AB. The zero-axis duty cycle is only changed and the durations of vectors U2 and U3 keep constant. Therefore, the controlled variables are not affected. It can be got that the variance of the zero-axis duty cycle is 6Δdk/kAB. The ZSCC controller design method of the line-side is identical with one of the generator-side.

V. SIMULATION ANALYSIS

This section presents the computer simulation of two parallel converters to validate the performance of the proposed topology and the control strategy. In other words, *n* is equal to two. It has

been done using *MATLAB/SIMULINK* simulation package. The specifications of the PMSG are shown in Table I. The PMSG operates at rated speed. The nominal line-to-line voltage of the three-phase grid is reduced to 230 V and the nominal grid frequency is 50 Hz. The PWM frequency is set at 5 kHz. The capacitances of the two dc capacitors are

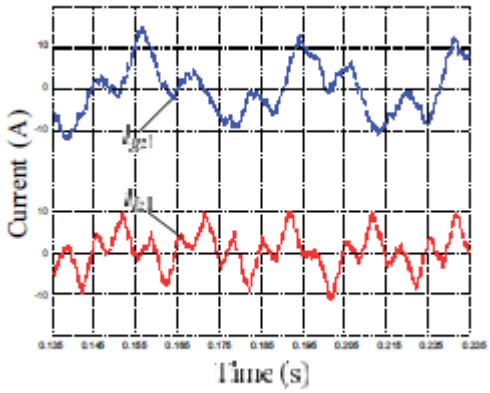

(a)

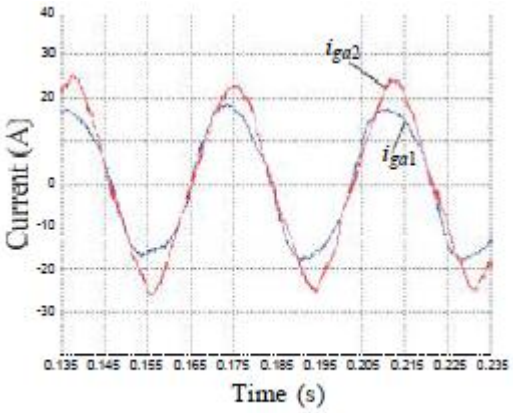

(b)

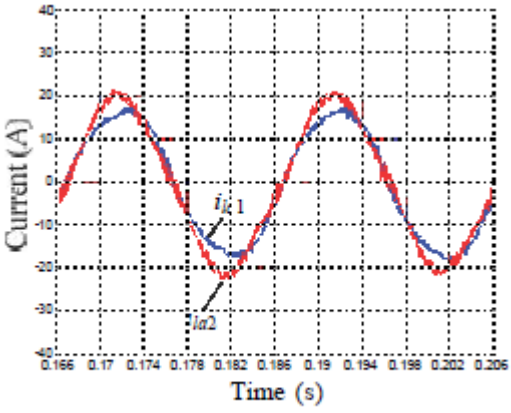

(c)

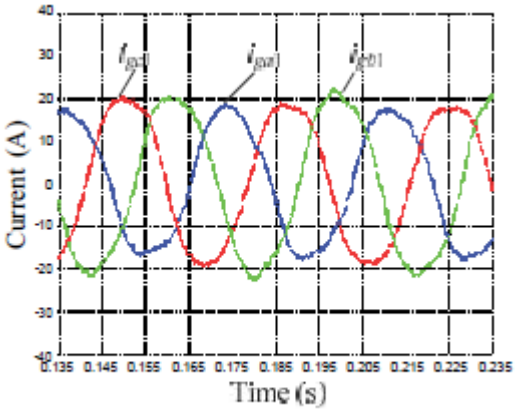

(d)

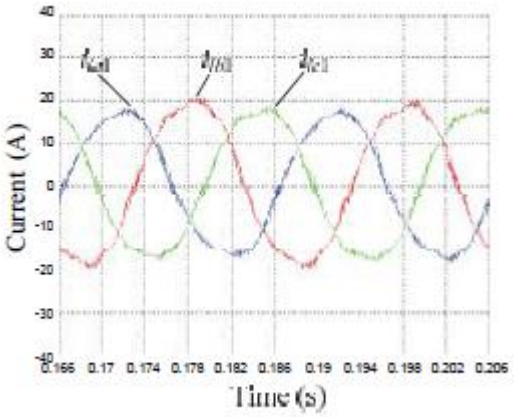

(e)

Fig. 8. Simulation waveforms without the ZSCC controllers. (a) ZSCCs of the 1*st* generator-side converter and the 1*st* line-side converter. (b) Phase A currents of the two generator-side converters. (c) Phase A currents of the two line-side converters. (d)Three-phase currents of the 1*st* generator-side converter. (e) Three-phase currents of the 1*st* line-side converter.

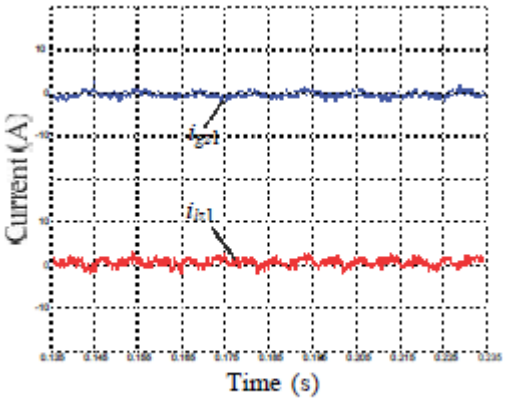

(a)

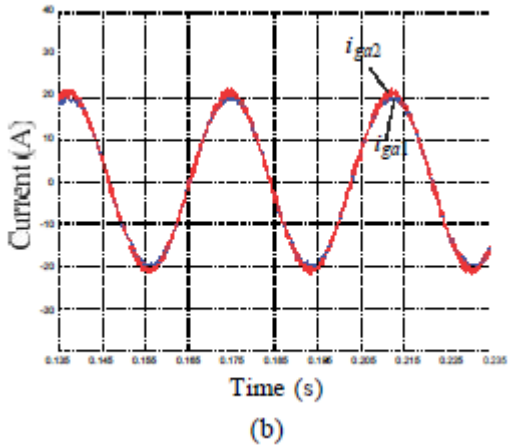

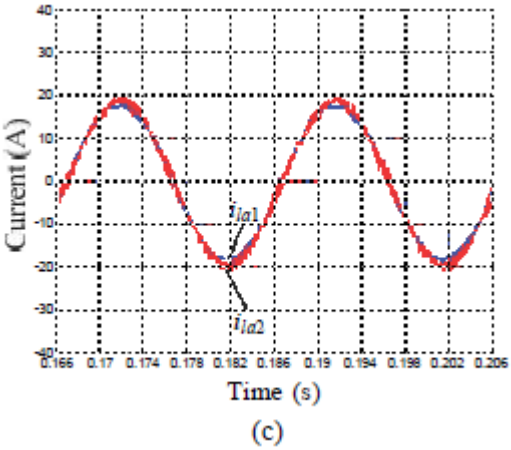

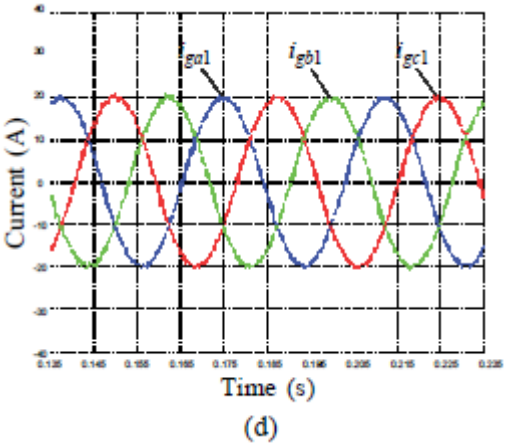

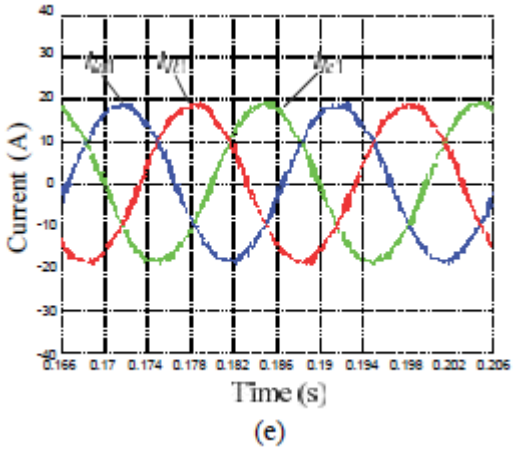

Fig. 9. Simulation waveforms with the ZSCC controllers. (a) ZSCCs of the 1st generator-side converter and the 1*st* line-side converter. (b) Phase A currents of the two generator-side converters. (c) Phase A currents of the two line-side converters. (d)Three-phase currents of the 1*st* generator-side converter. (e) Three-phase currents of the 1*st* line-side converter.

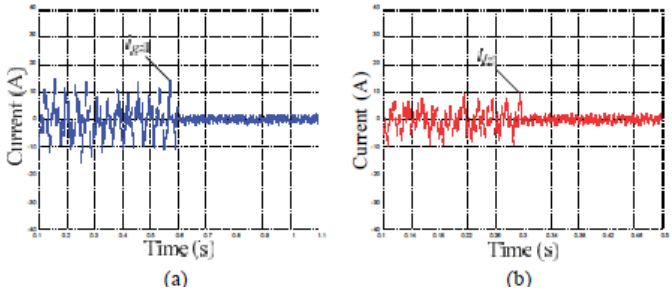

Fig. 10. Transient simulation waveforms. (a) ZSCC of the 1*st* generator-side converter. (b) ZSCC of the 1*st* line-side converter.

both 6800 μF and the voltage of the dc bus is 450 V. To simulate the character differences of the two parallel converters, some parameters are set differently. The inductances of the two generator-side inductors are set as 2.14 mH and 1.87 Mh respectively. The inductances of the two line-side inductors are set as 4.22 mH and 3.92 mH respectively. The dead-times of the two converters are 2.1 μs and 1.3 μs respectively. Besides, the 24 IGBTs used in the simulation have differences in internal resistance, forward voltage, fall time, and tail time, etc.

A. Simulation waveforms without the ZSCC controllers

Fig. 8 shows the simulation waveforms of the system without the ZSCC controllers. It can be seen from Fig. 8 (a) that the ZSCCs of the generator-side and the line-side are both serious. Fig. 8 (b) and (c) show that the current discrepancy and distortion is serious. It can be seen from Fig. 8 (d) and (e) that the three-phase currents are distorted and unsymmetrical.

B. Simulation waveforms with the ZSCC controllers

Fig. 9 shows the simulation waveforms of the system with the ZSCC controllers. We can see from Fig. 9 (a) that the ZSCCs of the generator-side and the line-side are both zero nearly, which validates the effectiveness of the proposed ZSCC controllers. It can be seen from Fig. 9 (b) and (c) that the current waveforms of

the two parallel converters are consistent and the problems of current discrepancy and distortion are overcome well. Fig. 9 (d) and (e) show that the three-phase currents of the generator-side and the line-side are sinusoidal and symmetrical.

C. Transient simulation waveforms

Fig. 10 (a) and (b) show the transient simulation waveforms of ZSCCs on the generator-side and the line-side respectively. Before the actions of the ZSCC controllers, the ZSCCs of the generator-side and the line-side are both serious. After the actions of the ZSCC controllers, they are both zero nearly.

VI. EXPERIMENTAL ANALYSIS

In order to verify the previous analysis further, the experiment has been carried out on a laboratory setup to test the performance of the system with the proposed topology and the control strategy. The generator-side converters and the line-side converters are both composed of two converters respectively. In other words, *n* is equal to two. The hardware setup is shown in Fig. 11.

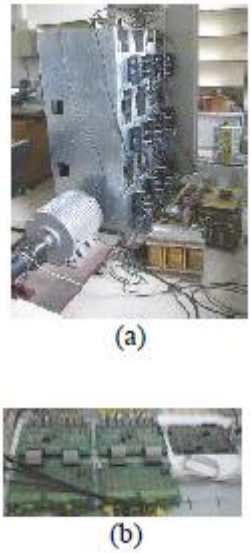

Fig. 11. Laboratory setup. (a) Main circuits. (b) Control circuits.

The specifications of the PMSG are identical with ones in the above simulation analysis which is shown in Table Ⅰ. The two generator-side converters are respectively connected to the PMSG through a three-phase inductor. The nominal inductance of the three-phase inductor is 2 mH and its accuracy is ± 10%. The capacitances of the two dc capacitors are both 6800 μF and the voltage of the dc bus is 450 V. The two line-side converters are respectively connected to the line through a three-phase inductor. Its nominal inductance is 4 mH and its accuracy is ± 10%. The nominal line-to-line voltage of the three-phase grid is reduced to 230 V and the nominal grid frequency is 50 Hz. The PWM frequency is set at 5 kHz. A 15 kW induction motor is used instead of wind turbine for the fast prototyping of system and makes the PMSG operate at rated speed. The adopted IGBT modules are the SEMIKRON SKiiP 2403GB172-4DW. The generator-side controller and the line-side controller have no differences, both of which have a fixed-point DSP TMS320F2812PGFA and a CPLD ALTERA MAX Ⅱ EPM570T100C5N. Besides, a master is used which has the function of communication and I/O.

A. Experimental waveforms without the ZSCC controllers

Fig. 12 shows the experimental waveforms of the system without the ZSCC controllers. We can see from Fig. 12 (a) that the ZSCCs of the generator-side and the line-side are both serious. Fig. 12 (b) and (c) show that the current discrepancy and distortion are serious. It can be seen from Fig. 12 (d) and (e) that the three-phase currents are distorted and unsymmetrical.

B. Experimental waveforms with the ZSCC controllers

Fig. 13 shows the experimental waveforms of the system with the ZSCC controllers. We can see from Fig. 13 (a) that the ZSCCs of the generator-side and the line-side are both suppressed well. It can be seen from Fig. 13 (b) and (c) that the current waveforms of the two parallel converters are consistent. Fig. 13 (d) and (e) show that the three-phase currents of the generator-side and the line-side are sinusoidal and symmetrical.

C. Transient experimental waveforms

Fig. 14 (a) and (b) show the transient experimental waveforms of ZSCCs on the generator-side and the line-side respectively. It can be seen that they are both zero nearly after the actions of the ZSCC controllers, which validates the

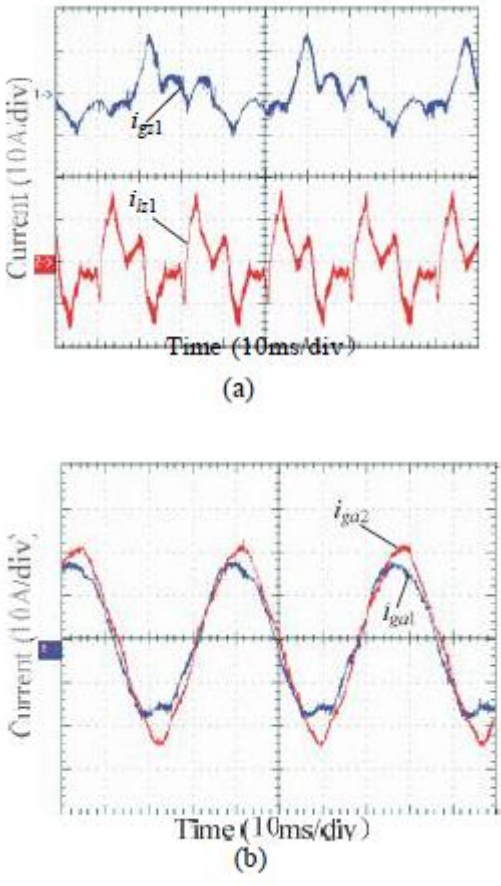

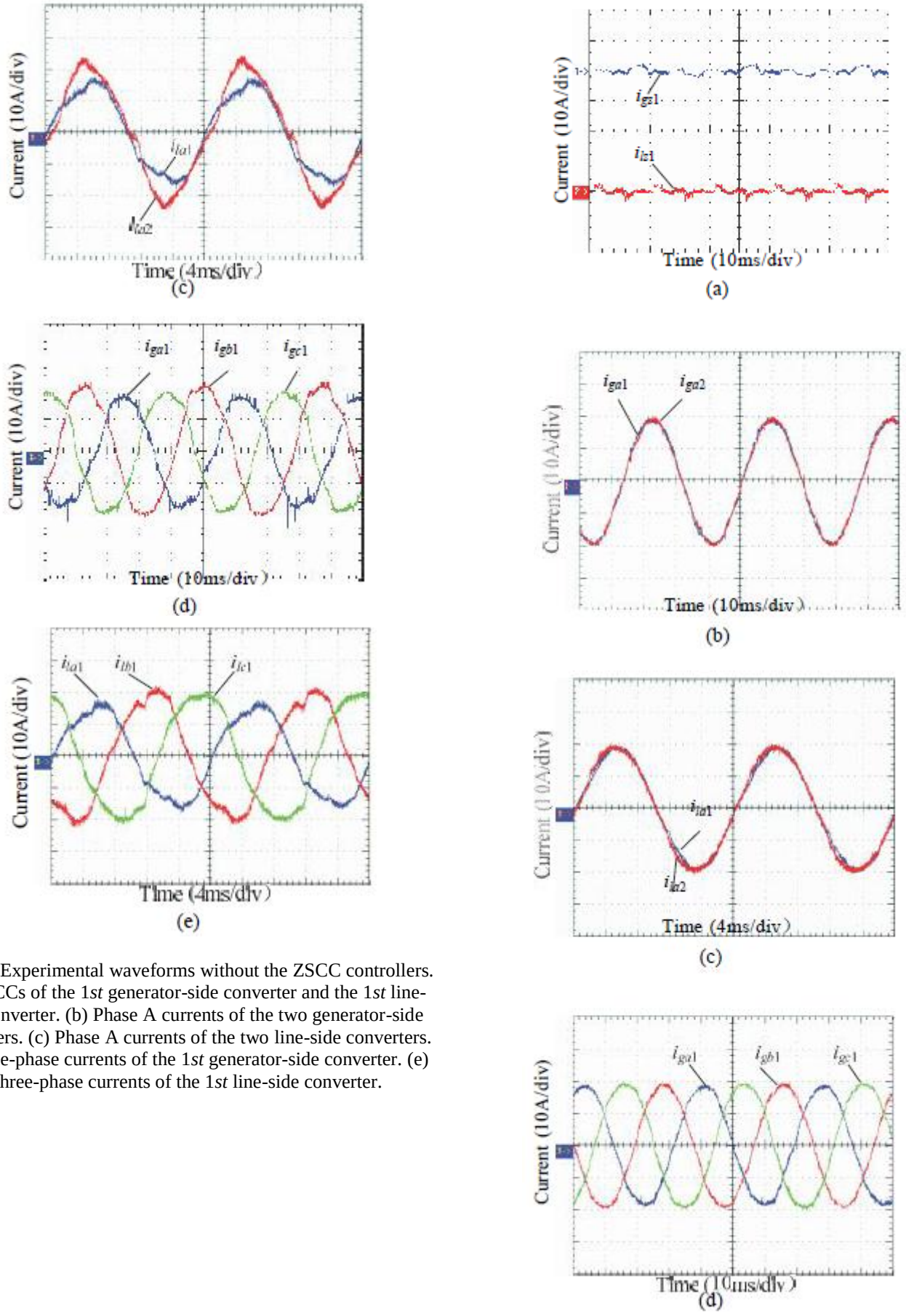

Fig. 12. Experimental waveforms without the ZSCC controllers. (a) ZSCCs of the 1*st* generator-side converter and the 1*st* line-side converter. (b) Phase A currents of the two generator-side converters. (c) Phase A currents of the two line-side converters. (d)Three-phase currents of the 1*st* generator-side converter. (e) Three-phase currents of the 1*st* line-side converter.

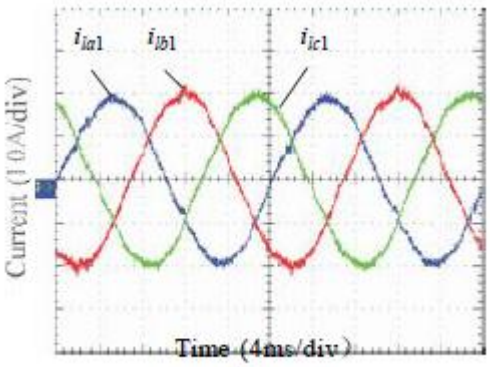

(e)

Fig. 13. Experimental waveforms with the ZSCC controllers. (a) ZSCCs of the 1*st* generator-side converter and the 1*st* line-side converter. (b) Phase A currents of the two generator-side converters. (c) Phase A currents of the two line-side converters. (d)Three-phase currents of the 1*st* generator-side converter. (e) Three-phase currents of the 1*st* line-side converter.

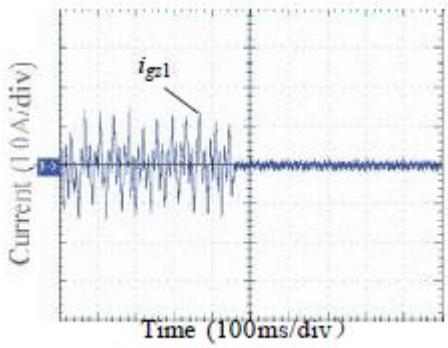

(a)

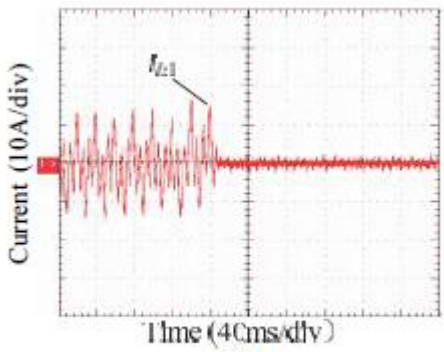

(b)

Fig. 14. Transient experimental waveforms. (a) ZSCC of the 1*st* generator-side converter. (b) ZSCC of the 1*st* line-side converter.

proposed control method of ZSCC. Besides, the experimental results are in accord with the above simulation ones.

VII. CONCLUSION

The paper proposes a new topology of PMDD wind power system which increases the power capacity of wind power converter effectively. It is found that the ZSCCs are caused by the discrepancy of zero-axis duty cycles of the parallel converters. Besides, the generator-side ZSCCs and the line-side ZSCCs are independent with each other. Therefore, the ZSCC controllers of the generator-side and the line-side can be designed independently. The proposed ZSCC controllers do not increase the hardware cost and have no effect on the controlled variables. Moreover, they do not change the conventional SVPWM strategy, which makes them easier to achieve and expands their application scope. They suppress the generator-side ZSCCs and the line-side ZSCCs effectively and the currents of parallel converters are sinusoidal and consistent. The problems of current discrepancy, distortion, and asymmetry are overcome well and the reliability and efficiency of the system are improved. The research results of the paper make it possible to manufacture the wind power converters with higher power rating.

APPENDIX

The mathematical equation for the SMO in two-phase stationary coordinates is got by (A-1):

$$\hat{\vec{i}}_{g1} = A\hat{\vec{i}}_{g1} + B(\vec{u}_{g1} - \hat{\vec{e}}_g - \vec{Z}) \quad \text{(A-1)}$$

Where

$$A = \begin{bmatrix} -R_e/L_e & 0 \\ 0 & -R_e/L_e \end{bmatrix} \; ; \quad B = \begin{bmatrix} -1/L_e & 0 \\ 0 & -1/L_e \end{bmatrix} \; ;$$

$$\vec{i} \quad \begin{bmatrix} \hat{i} \end{bmatrix} \quad \vec{u} \quad \begin{bmatrix} u \end{bmatrix} \; ; \quad \vec{e} \quad \begin{bmatrix} \hat{e}_{g\alpha} \end{bmatrix} \; ;$$

R and L are the

$$\hat{i} = \begin{vmatrix} g\alpha 1 \\ g\beta 1 \end{vmatrix} ; u = \begin{matrix} g\alpha \\ 1 \end{matrix} \quad \hat{e} = \begin{matrix} e \\ e \end{matrix}$$

$$\begin{matrix} g1 \\ \end{matrix} \begin{vmatrix} \hat{i} \\ \end{vmatrix} \begin{matrix} g1 \\ u \end{matrix} \begin{vmatrix} \\ \end{vmatrix} \begin{matrix} g \\ \hat{e} \end{matrix} \begin{vmatrix} \\ \end{vmatrix}$$

$$\begin{vmatrix} g\beta 1 \end{vmatrix} \quad \begin{vmatrix} g\beta 1 \end{vmatrix} \quad \begin{vmatrix} g\beta \end{vmatrix}$$

equivalent resistance and inductance of stator respectively; $\hat{}g\alpha$ 1 and $\hat{}ig\beta$ 1 are the α-axis and β-axis estimated currents; $ug\alpha 1$ and $ug\beta 1$ are the α-axis and β-axis reference voltages; $e\hat{}g\alpha$ and $e\hat{}g\beta$ are the α-axis and β-axis estimated EMFs of the PMSG. G Z is control signal and can be expressed as follows:

$$\vec{Z} = \begin{bmatrix} Z_\alpha \\ Z_\beta \end{bmatrix} \quad \text{(A-2)}$$

$$Z_\alpha = \begin{cases} -k, & s_\alpha \geq E_0 \\ -k\, s_\alpha / E_0, & |s_\alpha| < E_0 \\ k, & s_\alpha \leq E_0 \end{cases} \quad \text{(A-3)}$$

$$Z_\beta = \begin{cases} -k, & s_\beta \geq E_0 \\ -k\, s_\beta / E_0, & |s_\beta| < E_0 \\ k, & s_\beta \leq E_0 \end{cases} \quad \text{(A-4)}$$

Where

$s_\alpha = \hat{i}_{g1\alpha} - i_{g1\alpha}$; $s_\beta = \hat{i}_{g1\beta} - i_{g1\beta}$; $i_{g\alpha 1}$ and $i_{g\beta 1}$

α-axis and β-axis currents; $E0$ is the setting value of the current estimation error. The control signal Z is filtered with a first order low-pass filter and the estimated back EMF can be got:

$$\dot{\hat{e}}_g = -2\pi f_0 \hat{e}_g + 2\pi f_0 Z \quad \text{(A-5)}$$

where $f0$ is the cutoff frequency of the filter. Then the electrical rotor angular position of the PMSG θg can be obtained by (A-6):

$$\theta_g = -\tan^{-1}\left(\frac{\hat{e}_{g\alpha}}{\hat{e}_{g\beta}}\right). \quad \text{(A-6)}$$

REFERENCES

[1] S. Li and T. A. Haskew, "Characteristic study of vector-controlled direct driven permanent magnet synchronous generator in wind Power generation," in Proc. Power and Energy Society General Meeting, Pittsburgh, 2008, pp. 1–9.

[2] A. Yazdani and R. Iravani, "A neutral-point clamped converter system for direct-drive variable-speed wind power unit," IEEE Trans. Energy Convers., vol. 21, no. 2, pp. 596–607, Jun. 2006.

[3] M. Chinchilla, S. Arnaltes, and J. C. Burgos, "Control of permanent-magnet generators applied to variable-speed wind energy systems connected to the grid," IEEE Trans. Energy Convers., vol. 21, no. 1, pp. 130–135, Jun. 2006.

[4] M. A. Mueller, "Design and performance of a 20kW, 100rpm, switched reluctance generator for a direct drive wind energy converter," in Proc. IEEE Electric Machines and Drives Conf., San Antonio, 2005, pp. 56–63.

[5] J. Matas, M. Castilla, J. M. Guerrero, L. G. Vicuna, and J. Miret, "Feedback linearization of direct-drive synchronous wind-turbines via a sliding mode approach," IEEE Trans. Power Electron., vol. 23, no. 3, pp. 1093–1103, May. 2008.

[6] I. J. Gabe, V. F. Montagner, and H. Pinheiro, "Design and implementation of a robust current controller for VSI connected to the grid through an LCL filter," IEEE Trans. Power Electron., vol. 24, no. 6, pp. 1444–1452, Jun. 2009.

[7] M. Chinchilla, S. Arnaltes, and J. C. Burgos, "Control of permanent-magnet generators applied to variable-speed wind-energy systems connected to the grid," *IEEE Trans. Energy Convers.*, vol. 21, no. 1, pp. 130–134, Mar. 2006.

[8] T. P. Chen, "Circulating zero-sequence current control of parallel three-phase inverters," *IEE Proc. Electr. Power Appl*., vol. 153, no. 2, pp. 282–288, Mar. 2006.

[9] R. Turner, S. Walton, and R. Duke, "Stability and bandwidth implications of digitally controlled grid-connected parallel inverters," *IEEE Trans. Ind. Electron., vol. 57, no. 11, pp. 3685–3694, Nov. 2010.*

[10] L. Asiminoaei, E. Aeloiza, P. N. Enjeti, and F. Blaabjerg, "Shunt active-power-filter topology based on parallel interleaved inverters," IEEE Trans. Ind. Electron., vol. 55, no. 3, pp. 1175–1189, Mar. 2008.

[11] Y. Chen and K. M. Smedley, "One-cycle-controlled three-phase grid-connected inverters and their parallel operation," IEEE Trans. Ind. Applicat., vol. 44, no. 2, pp. 663–671, Mar./Apr. 2008.

[12] Z. H. Ye, D. Boroyevich, J. Y. Choi, and F. C. Lee, "Control of circulating current in two parallel three-phase boost rectifiers," IEEE Trans. Power Electron., vol. 17, no. 5, pp. 609–615, Sept. 2002.

[13] S. K. Mazumder, "Continuous and discrete variable-structure controls for parallel three-phase boost rectifier," IEEE Trans. Ind. Electron., vol. 52, no. 2, pp. 340–354, Apr. 2005.

[14] R. M. Cuzner, D. J. Nowak, A. Bendre, G. Oriti, and A. L. Julian, "Mitigating circulating common-mode currents between parallel soft-switched drive systems," IEEE Trans. Ind. Applicat., vol. 43, no. 5, pp. 1284–1294, Sept./Oct. 2007.

[15] T. P. Chen, "Dual-modulator compensation technique for parallel inverters using space-vector modulation," IEEE Trans. Ind. Electron., vol. 56, no. 8, pp. 3004–3012, Aug. 2009.

[16] F. S. Pai, J. M. Lin, and S. J. Huang, "Design of an inverter array for distributed generations with flexible capacity operations," IEEE Trans. Ind. Electron., vol. 57, no. 12, pp. 3927–3934, Dec. 2010.

[17] R. Ramos, D. Biel, E. Fossas, and F. Guinjoan, "Interleaving quasi-sliding-mode control of parallel-connected buck-based inverters," IEEE Trans. Ind. Electron., vol. 55, no. 11, pp. 3865–3873, Nov. 2008.

[18] J. Holtz, W. Lotzkat, and K. H. Werner, "A high-power multitransistor-inverter uninterruptable power supply system," IEEE Trans. Power Electron., vol. 3, no. 3, pp. 278–285, Jul. 1988.

[19] C. T. Pan, J. Y. Chang, C. M. Lai, Y. L. Juan, and Y. H. Liao, "Modeling of circulating currents for grid-connected parallel three-phase inverters," in Proc. SICE Annual Conf., Tokyo, 2008, pp. 1319–1322.

[20] L. L. Chen, L. Xiao, C. Y. Gong, and Y. G. Yan, "Circulating current's characteristics analysis and the control strategy of parallel system based on double close-loop controlled VSI," in Proc. IEEE Power Electron. Spec. Conf., Aachen, 2004, pp. 4791–4797.

[21] Y. Chen and K. M. Smedley, "Parallel operation of one-cycle controlled three-phase PFC rectifiers," IEEE Trans. Ind. Electron., vol. 54, no. 6, pp. 3217–3224, Dec. 2007.

[22] N. A. Rahim and J. Selvaraj, "Multistring five-level inverter with novel PWM control scheme for PV application," IEEE Trans. Ind. Electron., vol. 57, no. 6, pp. 2111–2123, Jun. 2010.

[23] W. Yao, M. Chen, J. Matas, J. M. Guerrero, and Z. M. Qian, "Design and analysis of the droop control method for parallel inverters considering the impact of the complex impedance on the power sharing," IEEE Trans. Ind. Electron., vol. 58, no. 2, pp. 576–588, Feb. 2011.

[24] S. K. Mazumder, "A novel discrete control strategy for independent stabilization of parallel three-phase boost converters by combining cpace-vector modulation with variable-structure control," IEEE Trans. Power Electron., vol. 18, no. 4, pp. 1070–1083, Jul. 2003.

[25] C. T. Pan and Y. H. Liao, "Modeling and coordinate control of circulating currents in parallel three-phase boost rectifiers," IEEE Trans. Ind. Electron., vol. 54, no. 2, pp. 825–838, Apr. 2007.

[26] M. Jones, S. N. Vukosavic, and E. Levi, "Parallel-connected multiphase multidrive systems with single inverter supply," IEEE Trans. Ind. Electron., vol. 56, no. 6, pp. 2047–2057, Jun. 2009.

[27] K. Xing, F. C. Lee, D. Borojevic, Z. H. Ye, and S. Mazumder, "Interleaved PWM with Discontinuous Space-Vector Modulation," IEEE Trans. Energy Convers., vol. 14, no. 5, pp. 906–917, Sept. 1999.

[28] C. T. Pan and Y. H. Liao, "Modeling and control of circulating currents for parallel three-phase boost rectifiers with different load sharing," IEEE Trans. Ind. Electron., vol. 55, no. 7, pp. 2776–2785, Jul. 2008.

[29] J. Holtz, W. Lotzkat, and K. H. Werner, "A high-power multitransistor-inverter uninterruptable power supply system," IEEE Trans. Power Electron., vol. 3, no. 3, pp. 278–285, Jul. 1988.

[30] J. L. Li, Z. G. Gao, S. J. Hu, X. B. Fu, and H. H. Xu, "Application of parallel back-to-back PWM converter on the direct-drive wind power system," Automation of Electric Power Systems, vol. 32, no. 5, pp. 59–62, Mar. 2008.

[31] Y. Komatsuzaki, "Cross current control for parallel operating three phase inverter," in Proc. IEEE Power Electron. Spec. Conf., Taipei, 1994, pp. 943–950.

[32] S. Fukuda and K. Matsushita, "A control method for parallel-connected multiple inverter systems," in Proc. Power Electron. and Variable Speed Drive Conf., London, 1998, pp. 175–180.

[33] G. H. B. Foo and M. G. Rahman, "Direct torque control of an IPM-synchronous motor drive at very low speed using a sliding-mode stator flux observer," IEEE Trans. Power Electron., vol. 25, no. 4, pp. 933–942, Apr. 2010.

[34] F. J. Lin, J. C. Hwang, P. H. Chou, and Y. C. Hung, "FPGA-based intelligent-complementary sliding-mode control for PMLSM servo-drive system," IEEE Trans. Power Electron., vol. 25, no. 10, pp. 2573–2587, Oct. 2010.

[35] Z. Xu, P. Y. Ge, and D. G. Xu, "High performance control of a permanent magnet wind power generation system using an adaptive sliding observer," in Proc. Power Electron. and Drive Systems Conf., Taipei, 2009, pp. 67–71.

[36] S. Z. Chen, N. C. Cheung, K. C. Wong, and J. Wu, "Integral sliding-mode direct torque control of doubly-fed induction generators under unbalanced grid voltage," IEEE Trans. Energy Convers., vol. 25, no. 2, pp. 356–368, Jun. 2010.

[37] Z. Xu and M. F. Rahman, "An adaptive sliding stator flux observer for a direct-torque-controlled IPM synchronous motor drive," IEEE Trans. Ind. Electron., vol. 54, no. 5, pp. 2398–2406, Oct. 2007.

AUTHORS

First Author – B.Gavaskar Reddy, Head & Associate Professor, Department of EEE, RK College of Engineering

Second Author – L.Maheswari, Associate Professor, Department of EEE, RK College of Engineering,Vijayawada.

Third Author – Rajagopal, Professor, Department of EEE, RK College of Engineering, Vijayawada

Fourth Author – K.Naga Jyothi, Department of ECE, Madina College of Engineering, Kadapa